INDIAN JOURNAL OF SCIENCE AND TECHNOLOGY

ORIGINAL ARTICLE

Electrochemical Detection of L-Ascorbic Acid and Photocatalytic Application of $Cu_5V_2O_{10}$ Nanomaterials

P Krishna Kaushik[1], J R Naveen Kumar[1]*, M Rohit[2], Divya R Basavannavar[2], B M Praveen[2], C Mallikarjunaswamy[3], R Harini[4], G Nagaraju[5]*, Bharath K Devendra[6]

1 Department of Electronics and Communication Engineering, Srinivas University Institute of Engineering and Technology, Mukka, Mangaluru, 574146, India
2 Department of Nanotechnology, Srinivas University Institute of Engineering and Technology, Mukka, Mangaluru, 574146, India
3 Department of Chemistry, JSS College Arts, Commerce and Science, Ooty Road, Mysuru, Kar-nataka, 570025, India
4 Department of Electronics and Communication Engineering, Govt. Polytechnic, Hiriyuru, Karnataka, 577527, India
5 Energy Materials Research Laboratory, Dept. of Chemistry, Siddaganga Institute of Technology, Tumakuru 572103, Karnataka, India
6 Department of Chemistry, M. S. Ramiah College of Arts, Science and Commerce-Autonomous, MSR Nagar, MSRIT Post, Bengaluru, Karnataka, 560054, India

OPEN ACCESS

Received: 23/12/2025

Accepted: 31/12/2025

Published: 22/01/2026

Citation: Krishna Kaushik P, Naveen Kumar JR, Rohit M, Basavannavar DR, Praveen BM, Mallikarjunaswamy C, Harini R, Nagaraju G, Devendra BK (2026) Electrochemical Detection of L-Ascorbic Acid and Photocatalytic Application of $Cu_5V_2O_{10}$ Nanomaterials. Indian Journal of Science and Technology 19(2): 95-106. https://doi.org/10.17485/IJST/v19i2.2014

* **Corresponding authors**.

naveenjr36@gmail.com

nagarajugn@sit.ac.in

Funding: None

Competing Interests: None

Copyright: © 2026 Krishna Kaushik et al. This is an open access article distributed under the terms of the Creative Commons Attribution License, which permits unrestricted use, distribution, and reproduction in any medium, provided the original author and source are credited.

Published By Indian Society for Education and Environment (iSee)

ISSN
Print: 0974-6846
Electronic: 0974-5645

Abstract

Objectives: The objective of this study was to develop an eco-friendly and multifunctional $Cu_5V_2O_{10}$ nanomaterial capable of addressing water pollution and electrochemical sensing challenges. The work aimed to synthesize CuVO nanoparticles using a green combustion method, evaluate their structural and optical properties, and explore their applicability in L-ascorbic acid sensing and photocatalytic dye degradation.

Methods: $Cu_5V_2O_{10}$ nanoparticles were synthesized via a green solution combustion route using *Salvia hispanica* seed powder as a bio-fuel, along with copper nitrate and ammonium metavanadate. The synthesis involved heating at 500 °C for 15 minutes followed by calcination at 600 °C for 3 hours. The nanoparticles were characterized using XRD, FTIR, PL, SEM, and UV-Vis spectroscopy. Electrochemical performance was investigated by modifying a glassy carbon electrode and studying its behavior using EIS, CV, and LSV. Photocatalytic activity was evaluated through the degradation of Rose Bengal dye under varying experimental conditions.

Findings: XRD confirmed the crystalline nature of $Cu_5V_2O_{10}$ nanoparticles, while SEM revealed porous, rod-like aggregated morphologies. Electrochemical studies showed enhanced electron transfer and effective detection of L-ascorbic acid, with CV and LSV responses increasing with scan rate and analyte concentration. The CuVO nanoparticles also exhibited excellent photocatalytic performance, achieving up to 98% degradation of Rose Bengal dye, with catalyst dosage, pH, and dye concentration playing significant roles.

Novelty: This study reports, for the first time, a *Salvia hispanica* seed powder–assisted green solution combustion route for the synthesis of phase-pure $Cu_5V_2O_{10}$ nanoparticles, eliminating the need for toxic fuels or surfactants. Beyond synthesis, the work uniquely establishes a single $Cu_5V_2O_{10}$ nanomaterial platform exhibiting dual functionality as both a highly sensitive electrochemical sensor and an efficient visible-light-driven photocatalyst. The synergistic enhancement in charge-transfer kinetics and photocatalytic activity, arising from the bio-assisted nanostructure and optimized crystallinity, leads to superior sensing performance and accelerated dye degradation compared to previously reported CuVO systems. This integrated demonstration of eco-friendly synthesis coupled with multifunctional environmental and electrochemical applications constitutes the key scientific advancement of the present work.

Keywords: Electrochemical sensing; Ascorbic acid; Rose Bengal; Photocatalysis; Impedance

1 Introduction

The development of functional nanoscale materials has attracted significant attention due to their exceptional physicochemical properties and wide-ranging applications in electrochemical sensing and environmental remediation. Among them, metal oxide nanoparticles such as ZnO, MnO_2, NiO, and CuO have been extensively explored as electrode modifiers owing to their high surface area, tunable electronic properties, and catalytic activity[1]. However, most reported studies have primarily focused on synthetic protocols and structural characterization, with comparatively limited emphasis on integrating green synthesis strategies with multifunctional performance evaluation[2],[3].

Electrochemical sensing platforms, particularly glassy carbon electrode (GCE)-based modified electrodes, have emerged as powerful analytical tools because of their high sensitivity, low cost, rapid response, portability, and ease of fabrication. Electrochemical techniques such as cyclic voltammetry (CV), electrochemical impedance spectroscopy (EIS), and linear sweep voltammetry (LSV) enable the detection of a wide range of biologically and environmentally relevant analytes[4]. Among these, L-ascorbic acid (vitamin C) is an essential biomolecule involved in antioxidant defense, iron absorption, immune response, and disease prevention. Accurate and reliable electrochemical detection of L-ascorbic acid remains crucial, yet challenges persist due to poor selectivity, electrode fouling, and sluggish charge-transfer kinetics in conventional sensing materials[5].

In parallel, the contamination of water bodies by synthetic dyes released from textile and industrial effluents poses a serious environmental and health threat. Azo and xanthene dyes, such as Rose Bengal, are particularly hazardous due to their toxicity, carcinogenicity, and resistance to biodegradation[6],[7],[8]. Although conventional wastewater treatment methods including adsorption, coagulation, membrane filtration, and ion exchange are effective, they often suffer from high operational costs, secondary pollution, and limited reusability. In this context, semiconductor-based photocatalysis has emerged as an environmentally benign and efficient alternative for dye degradation[9].

Recently, metal vanadates have gained increasing interest as photocatalysts and electrochemical materials because of their multiple oxidation states, oxygen vacancies, structural flexibility, and tunable band gaps[10]. Despite these advantages, the reported synthesis of vanadate nanomaterials frequently relies on energy-intensive, multi-step, or chemically harsh methods, limiting their sustainability and large-scale applicability. Moreover, studies that simultaneously explore the electrochemical sensing and photocatalytic performance of a single green-synthesized vanadate material remain scarce[11].

To date, there is a lack of eco-friendly synthesis routes that utilize biogenic fuels for producing multifunctional Cu–V–O nanomaterials, coupled with a systematic evaluation of their dual electrochemical sensing and photocatalytic capabilities. Specifically, the role of bio-assisted combustion synthesis in tailoring charge-transfer behavior, surface reactivity, and photocatalytic efficiency has not been adequately addressed[12].

In this study, we address these gaps by reporting a green solution combustion synthesis of $Cu_5V_2O_{10}$ nanoparticles using *Salvia hispanica* (chia seed) powder as a natural fuel, achieving a controlled crystallite size of 20.08 nm without toxic reagents. Structural and spectroscopic analyses confirmed Cu–O and V–O–V networks, favorable optical properties, and reduced charge recombination, enabling efficient electrochemical and photocatalytic performance. The key novelty lies in demonstrating a single green-synthesized $Cu_5V_2O_{10}$ nanomaterial with dual functionality. Compared to conventional Cu–V–O systems, the CuV NPs/GCE showed lower interfacial resistance (Rs = 781.7 Ω, Rct = 826.7 Ω) and surface-controlled electrocatalysis with strong linearity (R^2 = 0.9856) for L-ascorbic acid sensing. Additionally, 98% visible-light degradation of Rose Bengal within 180 min was achieved, driven by efficient charge separation and • OH radicals. Overall, green fuel-assisted combustion enables a scalable, eco-friendly multifunctional platform for sensing and wastewater remediation.

2 Methodology

2.1 Materials

chia seeds, *Salvia hispanica* are purchased from Tumkur, Karnataka, India. ammonium metavanadate, copper nitrate hexahydrate, ethanol, rose Bengal, methylene blue and L-ascorbic acid are purchased from MERCK. The ingredients were not purified before being utilized in the experiment.

2.2 Synthesis of NPs

A specific quantity of *Salvia hispanica* seeds was obtained and powdered after being finely ground. This served as fuel for all subsequent studies. Ammonium metavanadate, fuel, and copper nitrate hexahydrate were added to a crucible in a 1:1 ratio. After adding 10 milliliters of water, give it a 10-minute magnetic siting. The crucible is retained within the muffle furnace, which has been warmed to 500°C, following mixing. Afterwards, the crucible is removed and allowed to come to ambient temperatures. Next, it is roughly ground with a pestle and mortar. The material was heated to 600 °C for three hours. After cooling, the material was ground into an extremely fine powder for the sample.

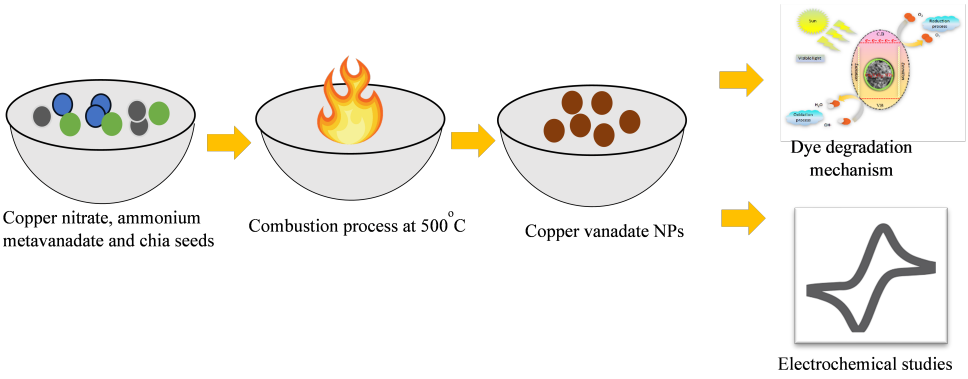


Fig 1. Synthesis process done through combustion

2.3 Preparation of copper vanadate modified glassy carbon electrode

The electrode (GCE/$Cu_5V_2O_{10}$) change was completed in accordance with earlier reports. Alumina was used to carefully polish the GCE (2 mm diameter) using a polishing cloth. To get rid of the deposited particles, the electrode was thereafter submerged in ethanol and sonicated. The drop cast process was used to coat the NPs. was demonstrated in **scheme 2**[13].

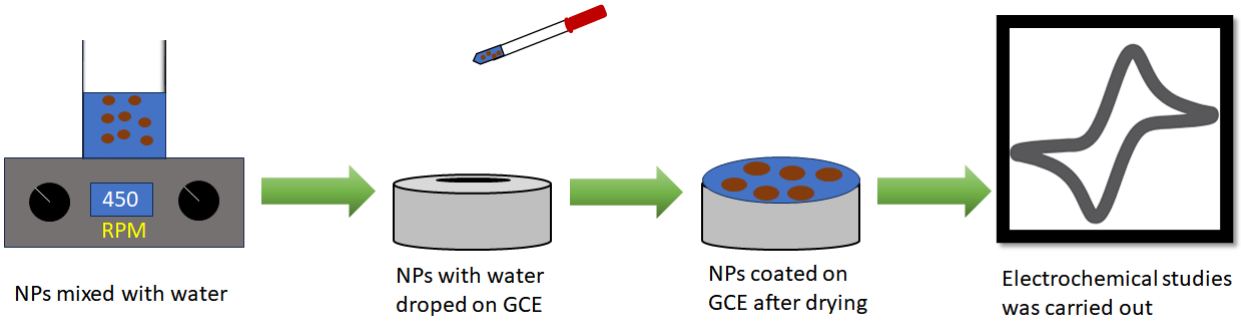


Fig 2. Modification of electrode for electro-chemical studies

2.4 Characterization

With the Rigaku Smart Lab X-ray diffractometer and CuKα radiation, the crystallographic geometry and content of Nanoparticles was ascertained. Utilizing a Bruker AlphaP spectrometer, the specimen's Fourier transform infrared (FTIR) spectrum is obtained. An Agilent ultraviolet-visible spectrophotometer was used for examining the specimen's absorbance spectrum. The Agilent Cary Eclipse was used to measure the photoluminescence (PL) spectra. NPs were examined using a JEOL JCM 6000 Plus a scanning electron microscope to determine their shape. Biologic sensing device, SP 50e.

2.5 Electrochemical impedance spectroscopy

Sensitive technique known as electrochemical impedance spectroscopy (EIS) may track how a system reacts to recurring, low-amplitude AC impulses. Different frequencies are used for EIS tests. Some information is included in the system response analysis, including the structure, interface, and reactions that take place.

2.6 Cyclic voltammetry

When using a potential scan, cyclic voltammetry (CV) is an effective technique for examining mechanism analysis of interfacial processes that take place on the electrode surface. The shift in current peaks can be used to measure the redox process of electroactive species. This allows for the quantitative determination of herbicide concentrations[14].

3 Photocatalytic dye degradation

Rose Bengal (RB) dye was selected as the catalyst's photocatalytic dye degradation (PCD) test material. 100 cc of water was mixed with 5 ppm of RB to create the dye solution. (HEBER photo reactor) with a 250W UV visible light source was utilized to degrade the dye. Samples were taken every 30 minutes for three hours while the solution was agitated in front of a light source. The following formula can be used to determine the percentage of RB dye degradation:

$$\% \text{ of dye removal} = \frac{Ci - Cf}{Ci} \times 100 \tag{1}$$

Where, Ci & Cf are the removal of RB of at time 0 & t, respectively.

4 Results and Discussion

4.1 X-ray diffraction Study

XRD examination of the produced NPs nanomaterial is shown in Figure 3(a), after calcination. Peaks of diffraction match JCPDS No. 70-1326. The diffraction peaks at 2θ= 27.40°, 28.70°, 32.60°, 33.64°, 36.75°, 38.05°, 40.13°, 41.96°, 45.94°, 54.06°, 55.09°, 59.52°, 64.45°, 65.50°, were indexed with the plane (210), (211), (114), (300), (-116), (123), (-221), (222), (320), (134), (-228), (208), (-521), (321),. The space group is Abam (no.14) with a=8.39300, b=6.05200, c=16.15600, and phase is monoclinic. Debye Scherrer's relation was utilized to determine the size of the crystallite.

$$D = \frac{k\lambda}{\beta \cos\theta} \tag{2}$$

Where λ is the wavelength of the X-ray used (1.54 x 10-10), B is the full width half-maximum (FWHM), D is the crystalline size, K is the diffraction constant (0.94), and θ is the angle of diffraction on X-ray incidence. The NPs' average crystallite size is 20.08nm. The atomic structure of $Cu_5V_2O_{10}$ is illustrated below in Figure 3(b).

4.2 Photoluminescence Study

The photoluminescence spectra of NPs are depicted in Figure 4(a, b). The excitation wavelength of $Cu_5V_2O_{10}$ NPs was 381 nm at room temperature, and the emission wavelength of $Cu_5V_2O_{10}$ NPs was 532 nm. One of the best methods for evaluating the efficiency of a semiconductor photocatalyst is the PL study, in which the involvement of the electron and holes are crucial. A high rate of electron-hole recombination reduces the photocatalytic activity. Therefore, the photocatalytic activity will be higher when the photoluminescence intensity is lower[15].

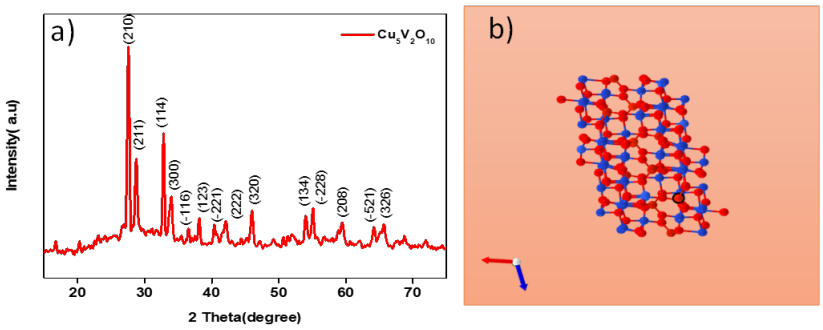


Fig 3. a) XRD of $Cu_5V_2O_{10}$ NPs. b) Atomic structure of $Cu_5V_2O_{10}$

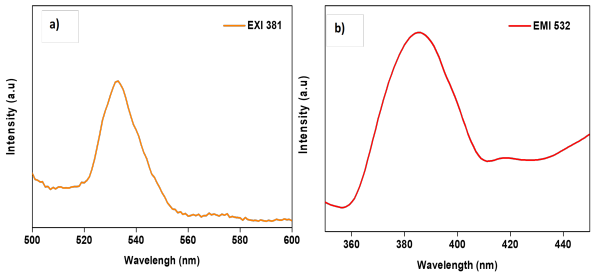


Fig 4. a) NPs was excited at 381nm to get a emission peak at 532nm, b) NPs was emitted at 532nm to get a emission peak at 381nm.

4.3 FTIR Study

Figure 4 displays the synthesized NPs' FTIR spectra. The peaks were measured between 400 and 4000 cm^{-1}. The bands between 3000 and 3600 cm^{-1} and the bending of the V-O to V=O bands found in a range of 500 to 1000 cm^{-1}, respectively, are probably caused by the adsorption water's hydrogen-bonded -OH groups. Figure 5 displays the synthesized NPs' measured FT-IR spectra. The spectrum shows that the synthesis of $Cu_5V_2O_{10}$ materials is indicated by the peaks at 3444, 2344, 1644, 1487, 1265, 1108, 940, 608, and 501 cm^{-1}. The absorption peaks, which can be seen at 3444, 2344, and 1644 cm^{-1}, corresponds with H–O and H–O–H's stretching and bending modes molecules, respectively, that are associated with attached water molecules. The antisymmetric stretching vibrations of V-O-V and the elongating vibration caused by V=O mode are in charge of the bands that formed at 1265, 1108, and 940 cm^{-1}, respectively. The stretching vibration of carbon dioxide is what causes the band that formed at 2344 cm^{-1}. Additionally, at 608 cm^{-1}, a symmetric stretching vibration of the b- $Cu_5V_2O_{10}$ chain oxygen bonds which are triply coordinated appeared. Additionally, the creation of copper vanadate nanorods was confirmed by the absorption bands at 608 and 501 cm^{-1}, which corresponded to Cu–O[16].

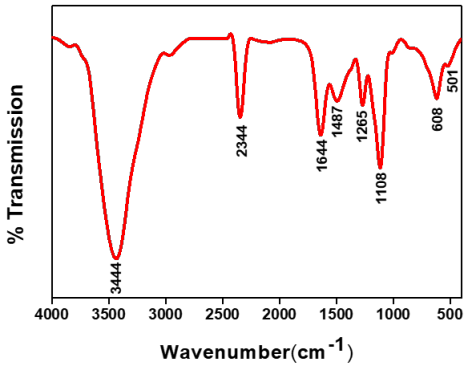


Fig 5. FTIR shows the functional group of NPs

4.4 Morphological analysis

The SEM analysis provides morphology of NPs which can be observed in Figure 6(a, b), which be represented as irregular with agglomeration. The images can be used to analyze the NPs at the range of 300nm to 10μm. EDX shows the presents of elements like vanadate, oxygen and copper.

4.5 UV-Visible Spectroscopy

To investigate the optical properties of the produced $Cu_5V_2O_{10}$ NPs, UV–Vis spectra is used. The Kubelka-Munk function was utilized to transform the reflectance spectrum into the absorbance spectrum, as demonstrated in **Eq. (3)** below:

$$F(R) = \alpha/S = (1-R)2/2R \tag{3}$$

wherein R is reflectance, S is the scattering coefficient, α is the absorption coefficient, and F(R) is the Kubelka-Munk function. The following formula can be used to estimate the bandgaps (Eg):

Figure 7(a) shows the ultraviolet (UV)-visible spectrum of $Cu_5V_2O_{10}$ NPs. The Kubelka-Munk function was utilized to compute the energy bandgap value.

$$(\alpha h\nu)2 = A(h\nu - Eg) \tag{4}$$

where A is the constant, hv is the energy of a photon, Eg is band gap energy, and α is the absorption coefficient. This formula gives us the amount of energy needed for our substance to lie within the spectrum of light. The synthesized material's predicted band gap energy is 1.85 eV (Figure 7b).

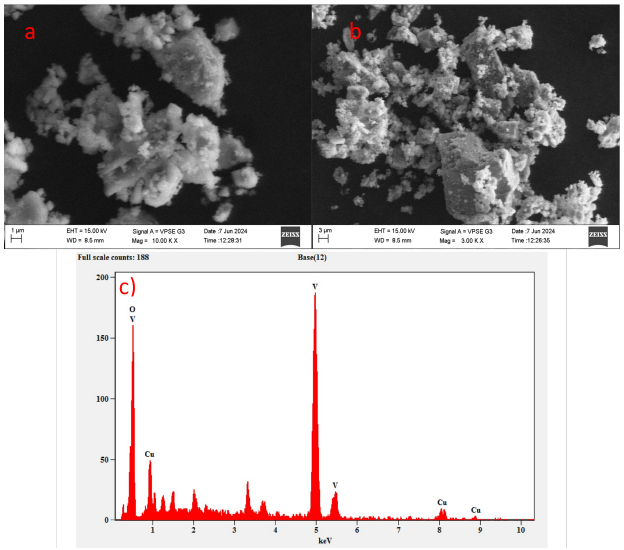


Fig 6. a, b) is SEM images of copper vanadate NPs, c) EDX showing the elements present in the copper vanadate nanoparticles

5 Electrochemical properties of NPs

5.1 Electrochemical Impedance Spectroscopy of NPs

Using the EIS method, the electrochemical performance of the as-synthesized CuV was examined. Figure 8a displays the Nyquist plots of the CuV electrode and the bare GCE. The experimental settings for the EIS test were set as follows: a signal voltage of 5 mV and a frequency band of 10 MHz to 100 kHz. The supportive electrolyte used for the evaluation was 0.1 M KCl. The resistance to charge transfers (R_{ct}) associated with the surface attribute is shown by the semi-circle at its lower frequency. The electrolytes solution's ionic resistance, R_s, and the Warburg impedance, Zw, make up the Randles equivalent circuit. The NPs/GCE, on the other hand, showed a Rs value of 781.7 ohm and a R_{ct} value of 826.7 ohm, accordingly. This indicates that the electrical modification was successful. Furthermore, the charge transfer resistance within the cathodic redox probe is increased

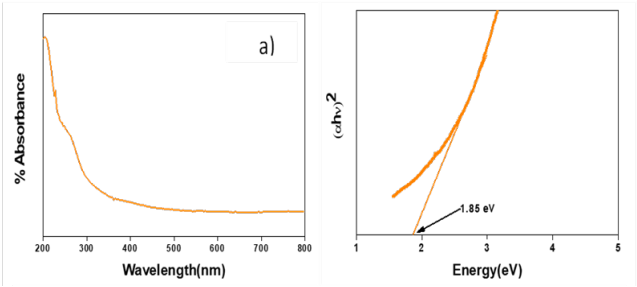


Fig 7. a) The wavelength of NPs using UB-Vis. b) The bandgap of NPS using Kubelka-Munk equation

by the existence of C–O–V bonds in vanadium oxide that link with –OH ions. It is possible that at less frequency, the ions in the electrolyte could enter the pores, causing a larger resistance. This finding further supports the successful modification of NPs on the electrode. The $C_1/(R_1+C_2/R_2+M_3)$ matches the equivalent randal circuit. C_1,C_2 represents the capacitance of the circuit, R_1,R_2, represents the resistance of the circuit, M represents the node in the circuit.

5.2 Electrochemical properties on CuV/GCE

To investigate the electrochemical behavior of the ($Cu_5V_2O_{10}$ NPs/GCE) modified GCE, I-V experiments were performed in distilled water solution in the presence of 10 μM L-Ascorbic acid (L-AA) as shown in Figure 8b. The current value with applied potential was clearly observed after L-AA injection. This is caused due to the direct oxidation and reduction of by L-AA.

The electrochemical performances of NPs modified GCE were analyzed using cyclic voltammetry (CV) experiments. Figure 8b shows the analysis of the impact of the scan rate using CV at different scan rates ranging from 20 to 100 mV s^{-1} in the presence of 10 μM L-AA containing distilled water[17].

It was investigated how the scan rate affected the anodic peak current of DA. The oxidation peak current (Ipa) rose with the scan rate. The anodic peak current increased from 55μA to 97μA. Throughout the 20–100 mV/s range, the Ipa was directly proportional to the scan rate (v). A surface-controlled procedure at the modified electrode surface was proposed in Figure 8b[18]. Throughout the 20–100 mV/s range, the decrease peak current (Ipc) from -25μA to -55μA was inversely related to the scan rate (v) (Figure 8b).

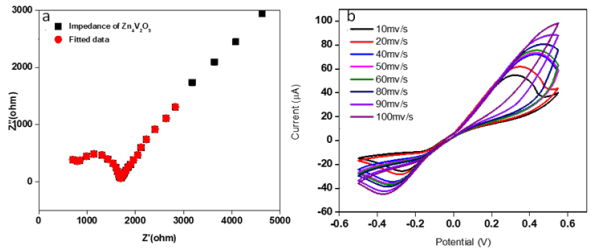


Fig 8. a) Impedance data with fitted data of Randals circuit. b) Cyclic voltammetry of NPs is distilled water for sending of ascorbic acid with different scan rate

5.3 Linear sweep voltammetry of L-AA

The varied concentrations of L-AA, ranging from 10 to 100 μM, were examined in distilled water at a scan rate of 50 mV s^{-1} in order to confirm the electrocatalytic activity of the CuV modified electrode. As the concentration of L-AA increases, as shown in Figure 9a, the peak steadily rises, indicating an effective electrocatalyst for the CuV modified GCE. The related linear plot of the decrease in peak current against the concentration of L-AA was shown in Figure 9b. This linear fit equation, which is represented as going from I_{pc}=(-34.75 μM) to I_{pc}=(-71.13 μM), has correlation coefficients. Additionally, the linear fit of the L-AA and current concentration plot (Figure 9b) is presented. R_2 = 0.9856 and y = 0.39818 indicate that first-order kinetics govern the total electro-reduction of L-AA at CuV/GCE.

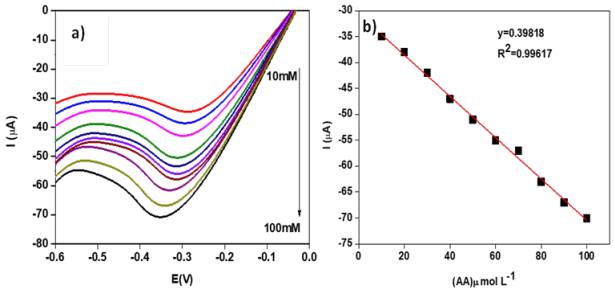


Fig 9. a) LSV profile of $Cu_5V_2O_{10}$/GCE in solution of pH7 with different concentration of L-AA, b) Linear regration of LSV with current vs concentration of L-AA

6 Photocatalytic degradation of RB dye

6.1 Comparison of cationic and anionic dye

For the degradation investigation of NPs there are two kinds of dyes used: anionic dye (Rose Bengal) and cationic dye (Rhodamine B). The structures of both cationic and anionic dyes are shown in Figure 9(a, b). Rhodamine-B (Rh-B) and Rose Bengal (RB) degradation was examined using two quartz tubes with the same dye concentration (5 ppm) and the same quantity of NPs (5 mg) in each dye. After the artificial NPs were added, RB was broken down more quickly than Rh-B. 180 minutes of photocatalytic degradation testing (Figure 10). Consequently, RB is used in further research.

6.2 Dye degradation mechanism

Anionic dyes like Rose Bengal (RB) are poisonous and utilized in the textile industry. It is essential that these colors break down. The material receives energy from visible light, which stimulates the valence band (VB) electrons, causing them to shift into the conduction band (CB), a higher band. In VB, oxidation results in the creation of holes, which then create hydroxyl radicals when they interact with water molecules. Superoxide radicals are created in CB when reduction occurs, and those electrons combine with oxygen molecules. The dye is degraded and rendered harmless by these reactive intermediates[18]. Scheme **??** depicts the process involved in dye degradation as well as the mechanism of RB dye degradation is depicted below.

$Cu_5V_2O_{10}$ + visible light ————– $Cu_5V_2O_{10}$ (e-cb + h+vb) (5)
$Cu_5V_2O_{10}$ (h+vb) + H2O ————- H+ + • OH (6)
$Cu_5V_2O_{10}$ (e-cb) + O2 ————- • O_2.- (7)
• O_2.- + H+ ———— • OH (8)
2e-cb + H+ ————- • OH + OH- (9)
$Cu_5V_2O_{10}$ (h+vb)+ HO- ————- • OH (10)
Organic pollutants + • OH ——- Degradation products (11)

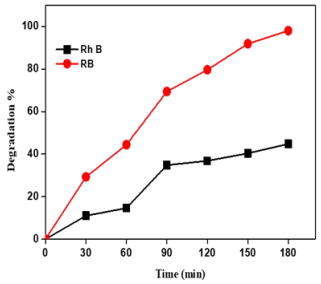


Fig 10. Comparison of photo catalytic degradation of RB and RnB

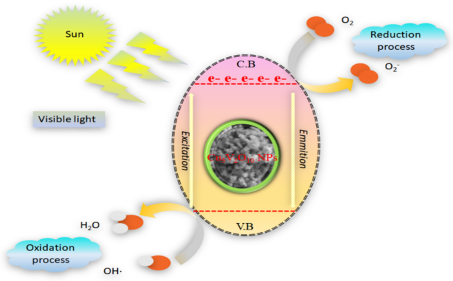


Fig 11. Dye degradation mechanism using $Cu_5V_2O_{10}$ NPs

Table 1. Represents the different materials with the comparison of the previous works and our research

Sl. No	Materials	Method	Dye	Degradation %	Ref.
1	TiO_2	Sol-gel	Acid red	93%	19
2	ZnO	Precipitation	Acid red	85%	
3	CdS	Microwave irradiation	Methylene blue	81%	20
4	ZnS	Microwave irradiation	Methylene blue	73%	
5	$BiVO_4$	Thermal decomposition method	Methylene blue	93%	21
6	ZnO embedded S-dopped g-C_3N_4	Sol-gel	Methylene blue	69%	22
7	CaO NPs (Plant Source)	Green combustion	Fast orange & Fast blue dyes	79.5%	23
8	V_2O_5/g-C_3N_4 nanocomposites	Solvothermal + ultrasonic	Rose Bengal, MB, Auramine O	85.1%	24
9	Ag@Cu/TiO_2 nanocomposites	Composite synthesis	Rose Bengal dye	81.07%	25
10	$Cu_5V_2O_{10}$	Solution combustion method	Rose bengal	98%	Current work

6.3 Effect of catalytic load

Determining the catalyst's photocatalytic efficacy requires figuring out the ideal catalyst load. Every 30 minutes, the impact of increasing the NPs' dosage on PCD was assessed. Figure 12(a) displayed the percentage of degradation after increasing catalyst loading from 5 mg to 20 mg. Up to 15 mg, the highest degradation rate is maintained, and after 20 mg, the degradation rate starts to decline. A larger number of dye molecules occupy the catalyst when additional catalyst is applied. Because less light will reach the metal oxide as a result, it will be less able to produce hydroxyl radicals. Based on the obtained results, the ideal catalyst load for degradation is 15 mg.

6.4 Effect of dye dosage

There were made dye solutions with concentrations ranging from 5 ppm to 20 ppm. In order to examine the impact of altering the initially set dye concentration, additional a predetermined amount (15 mg) of NPs to each dye solution. It was checked every 30 minutes, as Figure 12(b) illustrates. At 10 ppm, the deterioration percentage reaches its maximum. Because less hydroxyl radicals are attacking dye molecules, the rate of degradation decreases. The production of holes and the hydroxyl radicals that are released will remain steady when the ppm rises since there are always the same number of catalysts; however, the rate of degradation reduces with an increase of dye molecules [19].

6.5 Effect of pH concentration

NaOH and HCl solutions that were diluted were used to create pH solutions with a range of 3 to 11. The effect of a pH adjustment was investigated by adding predetermined catalyst and dye concentrations in each solution. It was checked as indicated in

Figure 12(c) every 30 minutes. The degradation percentage is highest at pH 7, and it is lower at pH 3, pH 5, and pH 11 than it is at pH 9. Because the semiconductor and dye are less repelled by one another, the degradation percentage falls as pH rises. However, at pH 9, there are less H^+ ions present, which prevents protonation, and there is less positive charge in semiconductors, leading to greater deterioration than at pH 3, pH 5, and pH 9[20].

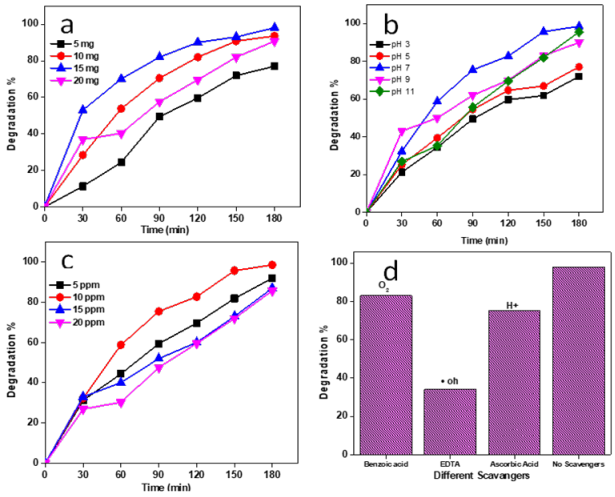


Fig 12. a) Effect of catalyst load NPs. b) Effect of different pH on degradation. c) Effect of different concentration of dye. d) Scavengers study for detection of radicals

6.6 Scavengers

We employed EDTA, ascorbic acid, and benzoic acid, which are responsible for masking the hydroxical radicals, to determine which hydroxical radicals are responsible for the dye degradation ·H, H+, and O^2. In line with the Figure 12(d). Since the EDTA molecules hide the NPs and prevent light from interacting with them, we can conclude that EDTA has a low degradation percentage because the dye cannot be broken down by the NPs.

6.7 Kinetic study

To determine the Rose Bengal dye's PCD kinetics, the Langmuir-Hinshelwood formula was applied. The equation is ln (Co/Ct)=kt, where k is the rate constant Co is the initial dye concentration at time 0 min, and Ct is the dye concentration at the specified time interval. RB's rate constant is 0.01106 min^{-1}, while Rh-B's rate constant is 0.0012 min^{-1}. As illustrated in Figure 13(a), photocatalytic degradation of dyes proceeds according to pseudo-first-order kinetics[21].

6.8 Reusability of catalyst

One crucial PCD application for dyes is the catalyst's reuse. Four successful recycling cycles of the catalyst resulted in a smaller decline in the degradation percentage. The ideal catalyst for this experiment is 15 mg. Centrifugation was used to recover the catalyst from the solution following each cycle, allowing it to be separated. For the second, third and four cycles, this was done again. The decline in the degradation % is depicted in Figure 13(b).

7 Conclusion

This study demonstrates a green and sustainable solution combustion synthesis of phase-pure $Cu_5V_2O_{10}$ nanoparticles using *Salvia hispanica* seed powder, achieving a controlled crystallite size of 20.08 nm without toxic reagents. Structural and spectroscopic analyses confirmed the formation of Cu–O and V–O–V networks with favorable optical properties and reduced charge recombination, supporting efficient electrochemical and photocatalytic behavior. The key novelty lies in establishing a single green-synthesized $Cu_5V_2O_{10}$ nanomaterial with dual functionality. Electrochemical studies, EIS analysis showed that the CuV NPs/GCE exhibited Rs = 781.7 Ω and Rct = 826.7 Ω, confirming successful electrode modification and enhanced charge-transfer kinetics. CV results raised the anodic peak current from 55 to 97 μA and the cathodic peak from –25 to

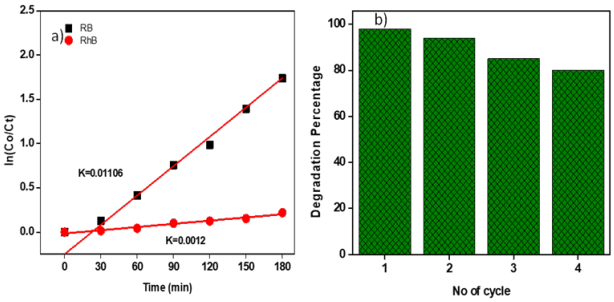


Fig 13. A) Kinetic study of RB and RhB. B) Reusability efficiency of $Cu_5V_2O_{10}$

–55 μA, indicating a surface-controlled electrochemical process and LSV with strong linearity (R^2 = 0.9856), confirming efficient electrocatalysis at the CuV/GCE. Concurrently, the nanoparticles exhibited 98% visible-light-driven degradation of Rose Bengal dye within 180 min, with hydroxyl radicals identified as the dominant reactive species. Inclusive, the results highlight $Cu_5V_2O_{10}$ nanoparticles as a cost-effective, eco-friendly, and multifunctional material for electrochemical sensing and wastewater remediation, with strong potential for practical deployment and further optimization through stability testing and material engineering.

References

1) Anantharama H, Kumar JN, Rohit M, Basavannavar DR, Praveen BM, Syed A, et al. Zinc vanadate nanoparticle: An innovative electrochemical sensor synthesized via green fuel for the detection of ascorbic acid and its other applications. *Journal of the Indian Chemical Society*. 2025;102(3):101607. 10.1016/j.jics.2025.101607.
2) Singh K, Yadav S. Biosynthesis of a range of ZnO nanoparticles utilising Salvia hispanica L. seed extract and evaluation of their bioactivity. *Scientific Reports*. 2025;15(1):4043. 10.1038/s41598-025-87355-3.
3) Asadian E, Ghalkhani M, Shahrokhian S. Electrochemical sensing based on carbon nanoparticles: A review. *Sensors and Actuators B: Chemical*. 2019;293:183–209. 10.1016/j.snb.2019.04.075.
4) Daniyal WMEMM, Fen YW, Kariming MZ, Fauzi NIM, Hashim HS, Anuar MF, et al. Enhanced surface plasmon resonance detection of ascorbic acid using carbon quantum dots thin film. *Plasmonics*. 2025;p. 1–12. 10.1007/s11468-025-03194-y.
5) Laschuk NO, Easton EB, Zenkina OV. Reducing the resistance for the use of electrochemical impedance spectroscopy analysis in materials chemistry. *RSC Advances*. 2021;11(45):27925–27936. 10.1039/D1RA03785D.
6) Arumugam S, Bavani T, Preeyanghaa M, Alaswad SO, Neppolian B, Madhavan J, et al. A facile synthesis of visible light driven Ni3V2O8 nano-cube/BiVO4 nanorod composite photocatalyst with enhanced photocatalytic activity towards degradation of acid orange 7. *Chemosphere*. 2022;308:136100. 10.1016/j.chemosphere.2022.136100.
7) Alharthi FA, Ababtain AS, Aldubeikl HK, Alanazi HS, Hasan I. Deep eutectic solvent-mediated synthesis of Ni3V2O8/N-doped RGO for visible-light-driven H2 evolution and simultaneous degradation of dyes. *Inorganics*. 2023;11(2):67. 10.3390/inorganics11020067.
8) Somashekar MN, Dhanalakshmi M, Nagamani TS, Chandra TS, Sharanakumar TM, Ravikumar CR. Photocatalytic and electrochemical sensor detection of ascorbic and uric acid using novel plant extract green synthesis of CaO nanoparticles. *Sensors International*. 2025;6:100308. 10.1016/j.sintl.2024.100308.
9) Xia D, Gao H, Li M, Gong F, Li M. Transition metal vanadates electrodes in lithium-ion batteries: a holistic review. *Energy Storage Materials*. 2021;35:169–191. 10.1016/j.ensm.2020.10.023.
10) Kumar EV, Swamy CM, Rao HA, Shashank M, Deepa K, Suma GR, et al. Facile green synthesis of CuWO4 nanoparticles and its application for the photocatalytic degradation of rose Bengal dye under visible light irradiation. *Inorganic Chemistry Communications*. 2025;172:113706. 10.1016/j.inoche.2024.113706.
11) Coban D, Tangal Y, Cogal S. MoSe2 nanosheets-based sensor for electrochemical detection of dopamine, ascorbic acid, and uric acid. *Journal of Materials Science: Materials in Electronics*. 2024;35(22):1513. 10.1007/s10854-024-13284-y.
12) Arumugam S, Bavani T, Preeyanghaa M, Neppolian B, Choi MY, Arunachalam P, et al. A novel Z-Scheme Ni3V2O8/AgI visible light photocatalyst with enhanced photocatalytic activity. 2023. 10.21203/rs.3.rs-3122756/v1.
13) Kumar AKS, Zhang Y, Li D, Compton RG. A mini-review: How reliable is the drop casting technique? *Electrochemistry Communications*. 2020;121:106867. 10.1016/j.elecom.2020.106867.
14) Du H, Xie Y, Wang J. Nanomaterial-sensors for herbicides detection using electrochemical techniques and prospect applications. *TrAC Trends in Analytical Chemistry*. 2021;135:116178. 10.1016/j.trac.2020.116178.
15) Chaman H, Alanazi SJ, Farooq MU, Nasir M, Andreescu S, Hayat A. Design of a Nano-Functionalized Lab-on-Paper Optical Sensing Platform for On-Site Detection of Ascorbic Acid in Natural Fruit Juices. *Applied Biochemistry and Biotechnology*. 2025;197(11):7464–7476. 10.1007/s12010-025-05403-0.
16) Venkadesh A, Mathew A, Fahmeeda TK, Sonia J, Kumara BN, Prasad KS. Paper Electrochemical Sensor Utilizing Nano Ag-Decorated Cu2O Nanoparticles for Ascorbic Acid Detection in Tablets. *Analysis & Sensing*. 2025;5(4):e202400118. 10.1002/anse.202400118.
17) Muthamizh S, Yesuraj J, Jayavel R, Contreras D, Varman KA, Mangalaraja RV. Microwave synthesis of β-Cu2V2O7 nanorods: structural, electrochemical supercapacitance, and photocatalytic properties. *Journal of Materials Science: Materials in Electronics*. 2021;32(3):2744–2756. 10.1007/s10854-020-05007-w.
18) Kesavan G, Vinothkumar V, Chen SM. Sonochemical synthesis of copper vanadate nanoparticles for the highly selective voltammetric detection of antibiotic drug ornidazole. *Journal of Alloys and Compounds*. 2021;867:159019. 10.1016/j.jallcom.2021.159019.

19) Kokila S, Nesaraj AS. Solar-Light Powered Photocatalytic Disintegration of Rose Bengal Dye Using Zn1-xMgxO1-δ–CuO–NiO Nanocomposites: Preparation, Functional Analysis and Optical Evaluation. *Journal of Inorganic and Organometallic Polymers and Materials*. 2025;p. 1–27. 10.1007/s10904-025-04138-z.
20) Rohit M, Reji R, Singh HN, Kumar JN, Alarfaj AA, Praveen BM, et al. Facile green synthesis of Ni3V2O8 nanoparticles for efficient photocatalytic degradation of Rose Bengal dye under visible light irradiation. *Chemical Physics Letters*. 2024;843:141246. 10.1016/j.cplett.2024.141246.
21) Basavannavar DR, Mishra KM, Biju A, Kumar JN, Praveen BM, Nagaraju G. Linum usitatissimum mediated green synthesis of Cu3V2O8 nanoparticles and its photocatalytic activity studies. *Environmental Nanotechnology, Monitoring & Management*. 2024;21:100912. 10.1016/j.enmm.2023.100912.